Transient Phenomena in Time- and Frequency-Gated Spontaneous Emission

Maxim F. Gelin,*,‡,§ Dassia Egorova,‡ Andrei V. Pisliakov,†,‡ and Wolfgang Domcke‡

Department of Chemistry, Technical University of Munich D-85747 Garching, Germany, and the Institute of Molecular and Atomic Physics, National Academy of Sciences of Belarus, Skaryna Avenue, 70, Minsk, 220072, Belarus

Received: December 6, 2004; In Final Form: February 23, 2005

The effect of overlapping pump and gate pulses on time- and frequency-gated spontaneous emission spectra is explored for a model of material dynamics that accounts for strong nonadiabatic and electron−vibrational coupling effects, vibrational relaxation, and optical dephasing, thus representing characteristic features of photoinduced excited-state dynamics in large molecules in the gas phase or in condensed phases. The behaviors of the sequential, coherent, and doorway−window contributions to the spontaneous emission spectrum are studied separately. The interrelation between the sequential and coherent contributions is demonstrated to be sensitive to the carrier frequencies of the pump and gate pulses and also to the optical dephasing rate, opening the possibility of an experimental determination of the latter. The coherent contribution is shown to dominate the spectrum at specific emission frequencies.

1. Introduction

The spontaneous emission (SE) spectrum is known to consist of two contributions, which can be termed as sequential (excitation precedes SE) and coherent (excitation and SE coexist in time). For steady-state SE spectra, a subtle interrelation exists between the two contributions, which depends crucially on the optical dephasing (OD) rate and is responsible for the partitioning of the SE into the fluorescence and resonance Raman parts.[1,2] If the SE is time-resolved, then the coherent contribution is important at short times (of the order of the duration of the excitation pulse), whereas the sequential contribution dominates the SE at longer times, when the processes of excitation and SE are well separated in time.[1−6] It is in this latter case that the time- and frequency-resolved SE spectra mirror the excited-state electronic population dynamics and vibrational wave-packet dynamics.[2,7,8]

To achieve temporal and spectral resolution of the SE simultaneously, one normally employs the so-called fluorescence up-conversion technique, passing the total emitted field through a spectrometer and a temporal gating device.[9,10] The spectra obtained in this manner are referred to as time- and frequency-gated (TFG) SE spectra.[4,11−15] From the theoretical point of view, the TFG SE signal can be represented as the sum of the doorway−window (DW) term, which determines the signal at those times at which the pump and gate pulses do not overlap any more, and the transient terms, which contribute to the signal at shorter times.[7,13,16]

Even with contemporary available laser pulses, the time interval during which the pulses overlap may spread over a few hundred femtoseconds. This time interval is not necessarily short on the time scale of the dynamics of the material system. For example, the solvation correlation functions extracted from the TFG SE spectra of dye LDS-750 in acetonitrile[17] and of coumarine in water[18] exhibit a sub-100-fs decay. The time-dependent cuts of the TFG SE spectra of several electron donor−acceptor complexes show coherent oscillations with a period of ∼150−200 fs.[19,20] Theoretical studies have also demonstrated that the effects due to the pump-gate pulse overlap affect the TFG SE peak-shift dynamics significantly.[7] Therefore, if one neglects the transient terms, then an interesting piece of the ultrafast system dynamics may escape detection. Moreover, the study of the TFG SE spectra in the domain of overlapping pulses can yield unique information about the onset and decay of various coherences (which give rise to complicated time-dependent interference patterns[21]) and may help to clarify the influence of this early stage of the evolution on the subsequent system dynamics.

It is well known that the short-time parts of pump−probe and other third-order spectroscopic signals with overlapping pulses contain information on the material system relaxation[8,22−43] being, in particular, sensitive to the OD rate and to the detuning of the pump−pulse carrier frequency. The results of these studies are not directly transferable to the TFG SE spectroscopy, however. Indeed, if the pump and probe pulses do not overlap, then the stimulated emission (excited state) contribution to the transient transmittance spectrum is equivalent to the TFG SE spectrum.[2,7,15] If the pulses overlap, then there is no such direct correspondence because the TFG SE spectrum contains both excited (sequential) and ground (coherent) contributions. Moreover, the coherent contribution to the pump−probe signal contains the sequence "probe−pump−pump−probe",[35] which does not contribute to the TFG SE spectrum.

The present study focuses on the exploration of the short-time behavior of TFG SE spectra, when the pump and gate pulses overlap and their durations are shorter than or comparable to the time scale of the system dynamics. To gain more insight, we study the problem analytically. A model of the material system has been chosen, which represents generic photoinduced excited-state dynamics in large molecules in the gas phase or

* Corresponding author. Present address: Department of Chemistry and Biochemistry, University of Maryland, College Park, MD 20742-4454.

† Present address: Department of Chemistry, University of California, Berkeley, CA 94720-1460.

‡ Technical University of Munich.

§ On leave from the Institute of Molecular and Atomic Physics, National Academy of Sciences of Belarus.

10.1021/jp044463t CCC: $30.25
Published on Web 04/02/2005

in condensed phases. It comprises the electronic ground state and two nonadiabatically coupled excited electronic states coupled to a harmonic reaction mode and thus accounts for strong nonadiabatic and electron−vibrational coupling effects. In addition, it includes vibrational relaxation, electronic population decay, and OD, which are described within a phenomenological relaxation model developed in ref 44.

2. Model

2.1. System Hamiltonian. We write the system Hamiltonian as the sum of an electronic ground-state Hamiltonian, H_g, and an excited-state Hamiltonian, H_e

$$H = H_g + H_e \tag{1}$$

To be more specific, we adopt a diabatic representation of the electronic states and express the Hamiltonians as

$$H_g = |g\rangle h_g \langle g| \tag{2}$$

$$H_e = \sum_{i=1}^{N} |i\rangle (h_i + \epsilon_i)\langle i| + \sum_{i \neq j}^{N} |i\rangle U_{ij} \langle j| \tag{3}$$

Here the bra-ket notation is used to denote diabatic electronic states; the summation indices in eq 3 run over all of the excited electronic states, and h_g and h_i denote the vibrational Hamiltonians pertaining to the ground and the excited states, respectively. ϵ_i is the vertical excitation energy of excited state $|i\rangle$ and U_{ij} are the nonadiabatic coupling matrix elements in the diabatic representation.

The transition dipole moment operator, which describes the coupling of the material system with the radiation field, is defined as follows

$$V \equiv V_{ge} + V_{eg},\ V_{ge} = V_{eg}^{\dagger} = \sum_{i=1}^{N} \xi_i |g\rangle\langle i| \tag{4}$$

so that the ground electronic state $|g\rangle$ is coupled radiatively with each excited state, $|i\rangle$, with ξ_i being the corresponding electronic transition dipole matrix element.

Throughout the article, we shall make use of the eigenvalue representation of the ground- and excited-state Hamiltonians

$$h_g|n\rangle = \epsilon_n|n\rangle \qquad H_e|\alpha\rangle = \epsilon_\alpha|\alpha\rangle \tag{5}$$

(hereafter, the eigenvalues and eigenfunctions of h_g and H_e are denoted by Latin and Greek letters, respectively). The corresponding transition frequencies are then defined as follows ($\hbar = 1$):

$$\omega_{\alpha n} = \epsilon_\alpha - \epsilon_n \qquad \omega_{\alpha\beta} = \epsilon_\alpha - \epsilon_\beta \qquad \omega_{nm} = \epsilon_n - \epsilon_m \tag{6}$$

We also introduce the quantities C_{ni}^{α}, which are the expansion coefficients of the excited-state vibronic eigenvectors in terms of the ground-state vibrational eigenvectors, $|\alpha\rangle \equiv \sum_{n,i} C_{ni}^{\alpha} |n\rangle|i\rangle$. Therefore, the matrix elements of the transition dipole operator in eq 4 are explicitly given as follows:

$$\langle g|\langle n|V_{ge}|\alpha\rangle \equiv V_{\alpha n} = \sum_{i=1}^{N} C_{ni}^{\alpha} \xi_i \tag{7}$$

Most of the analytical results obtained in the present article refer to the eigenvalue representation and are valid for any choice of H_g and H_e. For numerical illustrations, we shall use a model of excited-state electron transfer in the normal regime, which has been developed by Hayashi et al.[45,46] and implemented by the same authors as well as by Pisliakov et al.[47] for the interpretation of TFG SE experiments on the electron donor−acceptor complex TCNE-HMB by Rubtsov and Yoshihara.[19,20] The system Hamiltonian is given by eqs 2 and 3 with $N = 2$. The vibrational Hamiltonians, h_k (k = g, 1, 2), possess a single harmonic mode and are written in the second quantization representation as

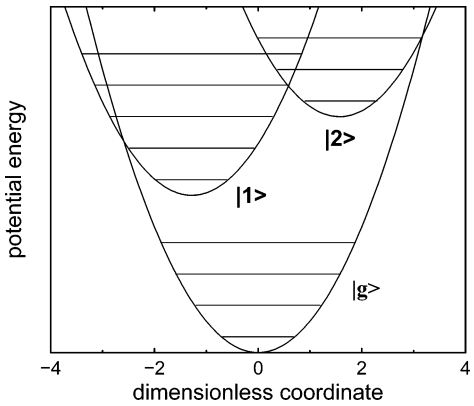

Figure 1. Schematic view of the potential energy surfaces of the model system.

$$h_k = \Omega\left\{b^{\dagger}b + {}^1\!/_2 - \frac{\Delta_k}{\sqrt{2}}(b^{\dagger} + b)\right\} \tag{8}$$

The reaction mode frequency, $\Omega = 0.0198$ eV, is assumed to be the same for all of the electronic states. The dimensionless horizontal displacements of the excited-state potential curves are the following: $\Delta_g = 0$, $\Delta_1 = -1.28$, and $\Delta_2 = 1.57$. The vertical excitation energies differ by $\epsilon_2 - \epsilon_1 = 0.0578$ eV so that the minima of the corresponding diabatic potential energy surfaces are shifted by $\approx 2.5\ \Omega$ (see Figure 1). The displacement of the minimum of the lower excited electronic state, $|1\rangle$, with respect to the minimum of the ground state, $|g\rangle$, has been put to zero, $\epsilon_1 - \Omega\Delta_1^2/2 = 0$. The electronic interstate coupling is of intermediate strength, $U_{12} = 0.007$ eV. The lower excited electronic state, $|1\rangle$, is assumed to be optically dark, whereas state $|2\rangle$ is optically bright, so that eq 7 reduces to $V_{\alpha n} = C_{n2}^{\alpha}$.

2.2. Phenomenological Relaxation Model. To account for various relaxation processes, we postulate the following kinetic equation for the system density matrix:

$$\partial_t \rho(t) = -\mathrm{i}[H - VE(t), \rho(t)] - (\Gamma_{el} + \Gamma_{vib})\rho(t) \tag{9}$$

Here, $E(t)$ is an external field, and the damping operators are defined as follows[44]

$$\Gamma_{el}\rho(t) = \xi_e P_e \rho(t) P_e + \xi_{eg}\{P_g \rho(t) P_e + H.c.\} \tag{10}$$

$$\Gamma_{vib}\rho(t) = \sum_{a=e,g} \nu_a P_a (\rho(t) P_a - \rho_a \{Tr P_a \rho(t)\}) \tag{11}$$

where

$$P_g = |g\rangle\langle g|,\ P_e = 1 - P_g \tag{12}$$

are the projection operators onto the ground and excited electronic states, and

$$\rho_a \equiv Z_a^{-1} \mathrm{e}^{-H_a/kT} \tag{13}$$

are the Boltzmann operators, with Z_a being the corresponding partition functions.

The damping operators, Γ_{el} and Γ_{vib}, are responsible for the electronic and vibrational relaxation, respectively. The first term in eq 10 reflects the excited-state population decay, with ξ_e being the corresponding rate. The second term in eq 10 is responsible for the OD (ξ_{eg} is the corresponding rate), which induces the decay of the optical coherences. Γ_{vib} has been introduced to ensure vibrational relaxation in each electronic state to its equilibrium form (13). The ν_a can thus be regarded as the vibrational relaxation rates.

Within the phenomenological relaxation model (9−11), one can derive explicit expressions for the third-order optical response functions $R_i(t_3, t_2, t_1)$,[44] which are collected in Appendix A.

3. TFG SE Spectrum

3.1. Response-Function Formalism. The TFG SE spectrum, which consists of the sequential (S) and coherent (C) contributions, can be expressed in terms of the third-order optical response functions as follows:[2,14,16]

$$S(t_0, \omega_0) = S^S(t_0, \omega_0) + S^C(t_0, \omega_0) \tag{14}$$

$$S^S(t_0, \omega_0) = Re\int_{-\infty}^{\infty} dt \int_0^{\infty} dt_3 \int_{-\infty}^{t_0+t} dt_2 \int_0^{\infty} dt_1 \; e^{(i\omega_0 - \gamma)t_3} E_L(t_2 - t_1)\, E_t(t + t_3)\, E_t(t)\, E_L(t_2) \; [R_1(t_3, t + t_0 - t_2, t_1) e^{i\omega_L t_1} + R_2(t_3, t + t_0 - t_2, t_1) e^{-i\omega_L t_1}] \tag{15}$$

$$S^C(t_0, \omega_0) = Re\int_{-\infty}^{\infty} dt \int_0^{\infty} dt_3 \int_t^{\infty} dt_2 \int_0^{\infty} dt_1 \; e^{-(\gamma - i\omega_0)t_3} E_L(t + t_0 - t_1)\, E_t(t)\, E_L(t_2 + t_0) \; E_t(t_3 + t_2)\, R_3(t_3, t_2 - t, t_1) e^{-i\omega_L t_1 + (i\{\omega_0 - \omega_L\} - \gamma)(t_2 - t)} \tag{16}$$

The frequency, ω_L, and the envelope, $E_L(t)$, characterize the excitation pulse, whereas ω_0 and $E_t(t)$ are the corresponding characteristics of the gate pulse. The parameter γ controls the spectral resolution, so that $\gamma = 0$ corresponds to an ideal frequency filter. The formulas (14−16) are valid provided that the excitation and the SE are treated in the lowest order of the perturbation theory with respect to system-field interaction and the rotating-wave approximation is employed (see ref 2 for details).

Note that the frequency-integrated SE signal

$$S(t) \equiv \int_{-\infty}^{\infty} d\omega_0\, S(t_0, \omega_0) \equiv \int_{-\infty}^{\infty} d\omega_0\, S^S(t_0, \omega_0) \tag{17}$$

is determined solely by the sequential term, (15), because as is evident from eq 16

$$\int_{-\infty}^{\infty} d\omega_0\, S^C(t_0, \omega_0) \equiv 0$$

This means that the coherent part at every particular t_0 contains, as a function of ω_0, both positive and negative contributions, which compensate each other upon integration. The overall signal, $S(t_0, \omega_0)$, is positive, of course.

Within the present article, the time-gate function and the excitation pulse envelope are chosen as exponentials

$$E_L(t) = \exp(-\Gamma_L|t|) \qquad E_t(t) = \exp(-\Gamma|t|). \tag{18}$$

This assumption is made frequently in the literature because it allows the derivation of analytical expressions.[4,16,22] It has been demonstrated that the substitution of Gaussian pulse envelopes by exponential pulse shapes does not give rise to qualitative differences in the time- and frequency-resolved spectra.[11,13] The implementation of the numerically exact method of paper[21] shows that this statement holds for overlapping time and gate pulses even beyond the limit of weak system-pump interaction.

3.2. Results and Discussion. In this section, we present explicit expressions for the TFG SE spectrum that are obtained by employing the phenomenological relaxation model for the third-order optical response functions (Appendix A), the eigenvalue representation for the ground- and excited-state Hamiltonians, and exponential envelopes (see eq 18) for the pump and gate pulses. To get a better understanding of the role of transient effects, we consider cuts of the TFG SE spectra calculated for the model system introduced in section 2. In particular, we examine how the signal is affected by the vibrational relaxation (ν_e), OD (ξ_{eg}), the durations of the pump and the gate pulses ($^1/_{\Gamma_L}$ and $^1/_{\Gamma}$) and, finally, by the carrier frequency (ω_L) of the pump pulse.

In the case of a CW pump pulse with a carrier frequency of the order of the vertical excitation energy, a few neighboring vibronic levels with large Franck−Condon factors are excited. When ω_L is increased, higher-lying vibronic levels with smaller Franck−Condon factors are populated. For the material system under study, the vertical excitation energy of the bright state is $\epsilon_2 \approx 3.7\ \Omega$. Thus, excitation by a pump pulse with the carrier frequencies of $\omega_L = 4$, 8, and 12 Ω will be referred to as the cases of small, moderate, and large detuning, respectively. The carrier frequency of the pump pulse used in the TFG SE measurements reported in refs 19 and 20 corresponds to $\omega_L = 11.5\ \Omega$.

Because we concentrate on the study of ultrafast phenomena, the pulse durations are chosen to be short on the vibrational dynamics time scale, and the lifetime of the excited state has been taken as infinitely large ($\xi_e = 0$). The temperature has been put to zero to emphasize coherent effects. A perfect spectral filter ($\gamma = 0$) has been assumed in all of the calculations.

3.2.1. Arbitrary Pump Pulse and Short Gate Pulse. First, we consider the situation when the gate pulse is short on the system dynamics time scale. In this case, the coherent contribution to the TFG SE spectrum, eq 16, can be neglected as compared to the sequential one, eq 15. Omitting the transient terms decaying with the characteristic time of the gate pulse, while keeping the transient terms decaying with the characteristic time of the pump pulse, one arrives at the generalized DW formalism.[16] As is shown in detail in Appendix B, the TFG SE spectrum can be calculated analytically and represented as the sum of the DW contribution ($S_{DW}(t_0, \omega_0)$) and the transient terms

$$S(t_0, \omega_0) \approx \theta(-t_0)\sum_{\alpha,\beta} \kappa^-_{1,\alpha\beta} \exp\{2\Gamma_L t_0\} + \theta(t_0)\Big(S_{DW}(t_0, \omega_0) + \sum_{\alpha,\beta}\{\kappa^+_{1,\alpha\beta}\exp\{-2\Gamma_L t_0\} - \sum_n \kappa^+_{2,\alpha\beta}(n)\exp\{-(\bar{\Gamma}_L - i\omega^L_{\alpha n})t_0\}\}\Big) \tag{19}$$

Here, $\theta(t)$ is the Heaviside step function, the quantities $\bar{\Gamma}^L$ and $\omega^L_{\alpha n}$ are defined via eq B16, and $\kappa^{\pm}_{x,\alpha\beta}$ are time-independent coefficients, the explicit form of which can be retrieved from eqs B10−13. The decay rates of the transient terms are seen to be determined by the duration of the pump pulse, $^1/_{\Gamma_L}$, and by the OD rate, ξ_{eg}, but are independent of the vibrational relaxation rate, ν_e, and the lifetime in the excited state, ξ_e. At negative times, the signal exhibits a monotonic onset, $\sim\exp\{2\Gamma_L t_0\}$. This

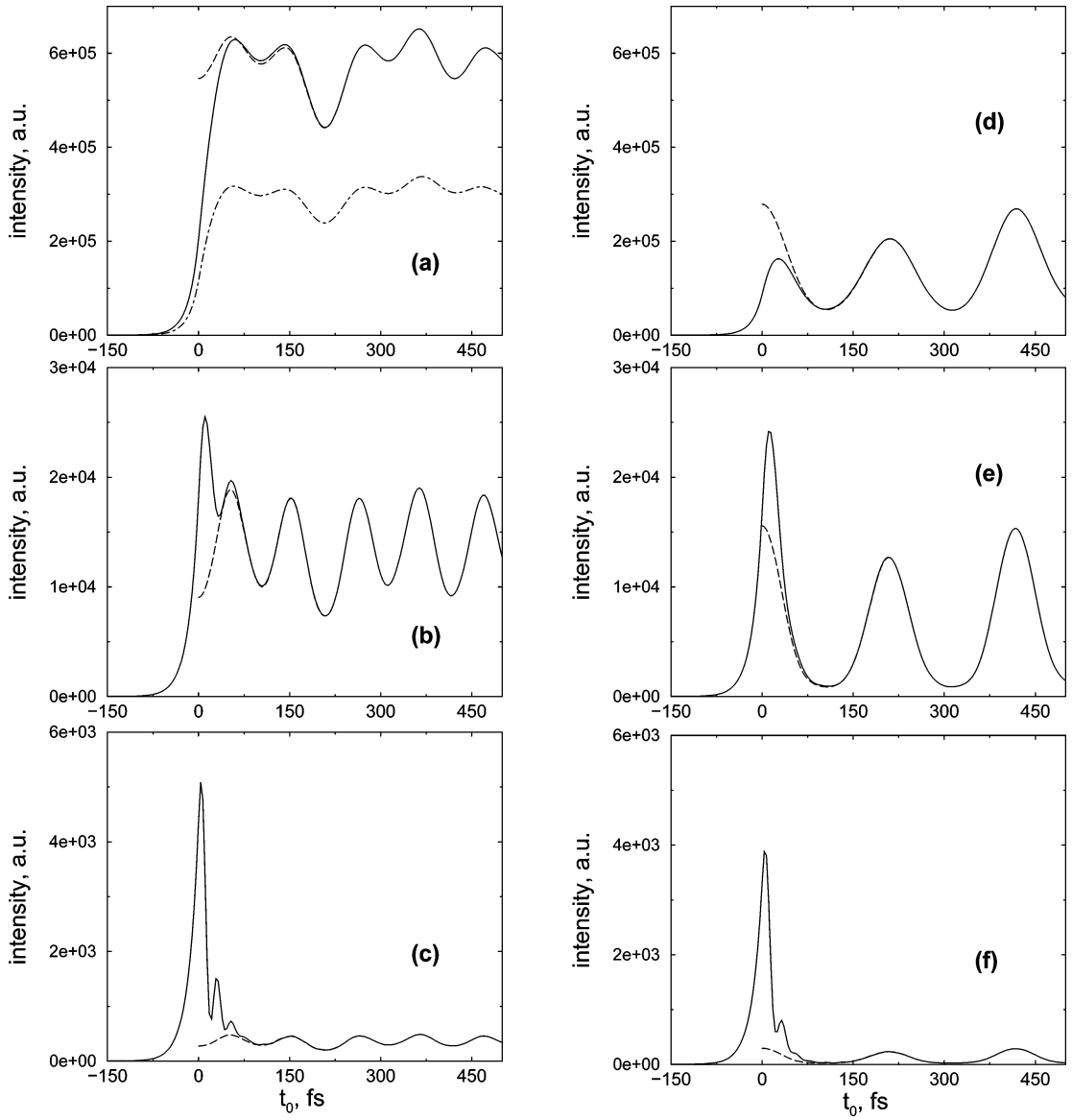

Figure 2. TFG SE spectra, calculated without dissipative effects, $\xi_{eg} = \nu_e = 0$. The inverse durations of the pump and gate pulses are $\Gamma_L = \Omega$ and $\Gamma = 5\ \Omega$, respectively. Shown are the cuts at the central frequency ($\omega_0 = \Omega$ in a−c) and in the wing of the fluorescence spectra ($\omega_0 = 8\ \Omega$ in d−f) for the cases of small, moderate, and large detunings. (The carrier frequency of the pump pulse is $\omega_L = 4\ \Omega$ in a and d, $\omega_L = 8\ \Omega$ in b and e, and $\omega_L = 12\ \Omega$ in c and d.) The solid lines show the exact (generalized DW) results, and the dotted lines show the results of the standard DW theory. The dot-dashed curve in Figure 2a is computed with the same parameters as above but with $\xi_{eg} = \Omega$.

onset follows (the square of) the excitation pulse envelope.[3,4] The evolution of the signal at positive times is described by the sum of the DW contribution and the transient terms. The term that is proportional to $\exp\{-2\Gamma_L t_0\}$ mirrors the signal onset. The second term is proportional to $\exp\{-(\bar{\Gamma}_L - i\omega^L_{\alpha n})t_0\}$. It exhibits, in general, an oscillatory behavior due to the presence of the vibronic frequencies $\omega^L_{\alpha n}$, and its magnitude is controlled by the two parameters, ξ_{eg} and Γ_L.

Let us try to get a more detailed view of typical scenarios of TFG SE spectra for the case of short gate and arbitrary pump pulses. To fulfill the conditions of the generalized DW approximation, we assume an excellent time resolution ($\Gamma = 5\ \Omega$), and the inverse duration of the pump pulse is given by $\Gamma_L = \Omega$.

The time-dependent cuts of the TFG SE spectra calculated without dissipative effects ($\xi_{eg} = \nu_e = 0$) are presented in Figure 2. The upper, middle, and lower panels correspond to the carrier frequencies $\omega_L = 4\ \Omega$ (Figure 2a and d), $\omega_L = 8\ \Omega$ (Figure 2b and e), and $\omega_L = 12\ \Omega$ (Figure 2c and f), respectively. The left column (Figures 2a−c) shows the cuts at a central frequency of the fluorescence spectrum ($\omega_0 = \Omega$), whereas the cuts in the wing ($\omega_0 = 8\ \Omega$) are shown in the right column (Figure 2d−f). The exact (generalized DW) results are given as full lines, whereas the approximate (standard DW) results are shown by dashed lines.

As expected, at $t_0 > 1/\Gamma_L$, when the transient terms vanish, the standard and generalized DW calculations coincide. The cuts in the wing (right column in Figure 2) exhibit oscillations with the fundamental vibrational period of $2\pi/\Omega = 209$ fs, whereas the cuts at the central frequency (left column in Figure 2) show beatings with a period of approximately π/Ω. This phenomenon is well known (see, for example, refs 61−63), being a manifestation of the fact that the wave packet moves over the potential minimum twice per period. In Figure 2a, b, d, and e, one also can see slower oscillations with a period of ∼410 fs that are superimposed on the vibrational beatings and represent electronic coherences caused by the electronic coupling, U_{12}. Accidentally, the period of these electronic beatings is about twice the vibrational period in the present model.

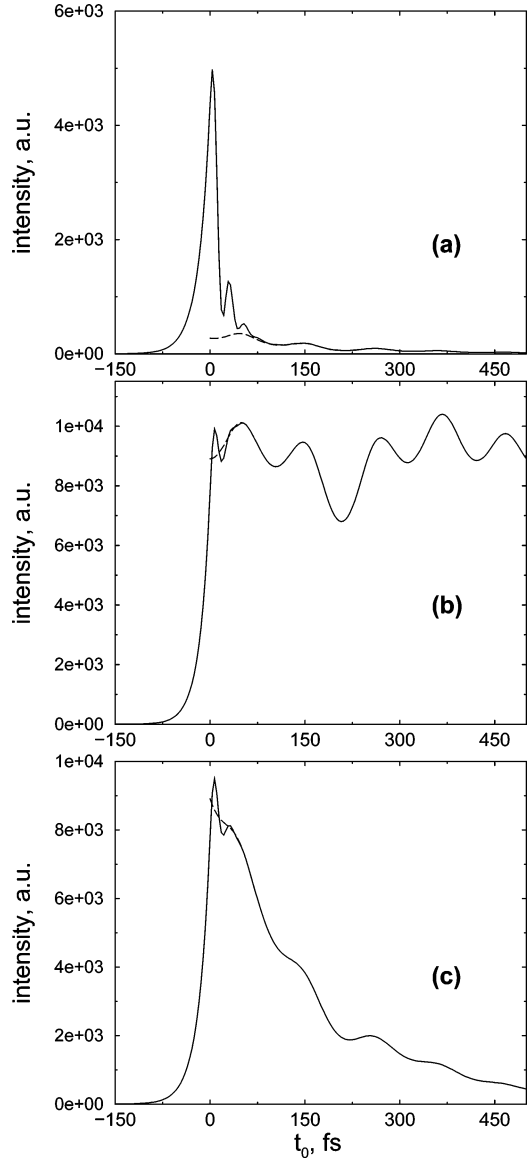

Figure 3. Cuts of the TFG SE spectrum calculated with the same parameters as in Figure 2c but taking into account dissipative effects. (a): $\nu_e = \Omega/3$, $\xi_{eg} = 0$; (b): $\xi_{eg} = \Omega$, $\nu_e = 0$; (c): $\xi_{eg} = \Omega$, $\nu_e = \Omega/3$. The solid lines show the exact (generalized DW) results, and the dotted lines show the results of the standard DW theory.

The increase of the carrier frequency, ω_L, does not lead to any significant changes of the long-time behavior but results in the overall intensity loss. Of our primary interest, however, is the short-time ($|t_0| < 1/\Gamma_L$) behavior of the cuts. One can clearly see an onset $\sim\theta(-t_0)\exp\{2\Gamma_L t_0\}$of the exactly calculated signal. If the pump−pulse frequency detuning is small, then the exact and DW cuts at the central frequency differ only slightly (Figure 2a), whereas those in the wing of the spectrum may differ by a factor of 2 (Figure 2d). If the pump-frequency detuning increases (middle panel, Figure 2b and e), then the cuts start to develop a peak in the vicinity of $t_0 \approx 0$ (compare with ref 56). The ratio of the peak intensity to the overall intensity of the signal at longer times increases with detuning and, for $\omega_L = 12\ \Omega$, reaches a value of ~10 (lower panel, Figure 2c and f).

The influence of the environment on the TFG SE spectra is illustrated in Figure 3. The cuts are calculated with the same parameters as in Figure 2c ($\omega_0 = \Omega$, $\Gamma_L = \Omega$, $\omega_L = 12\ \Omega$) as well as with vibrational damping ($\nu_e = \Omega/3$ and $\xi_{eg} = 0$ in Figure 3a) or OD ($\xi_{eg} = \Omega$ and $\nu_e = 0$ in Figure 3b). The combined effect of vibrational relaxation and OD ($\xi_{eg} = \Omega$, $\nu_e = \Omega/3$) is shown in Figure 3c. As is clearly seen from the comparison of Figures 2c and 3a, the detuning-induced peak in the vicinity of $t_0 \approx 0$ is unaffected by vibrational relaxation. The latter damps vibrational and electronic coherences and induces a decrease of the overall signal.[48] As for the OD, it reduces the height of the peak at $t_0 \approx 0$, thereby improving the quality of the DW description (Figure 3b and c).

Note that the influence of the OD on the TFG SE spectrum can turn from an overall decrease of the signal intensity, if the pump−pulse frequency detuning is small (the dot-dashed curve in Figure 2a has been computed with the same parameters as the solid line in this figure, but for the OD rate $\xi_{eg} = \Omega$), to an enhancement of the signal, if the detuning is high (compare Figures 2c and 3b). This is a realization of the turnover behavior that has been studied in more detail elsewhere.[21,49−55] However, the cut in Figure 3b resembles the cut in Figure 2a (dot-dashed curve) very much, although the intensities of the two differ dramatically. This indicates that the OD renders the shape of the cut, in contrast to its magnitude, much less sensitive to the pump−pulse carrier frequency detuning.

The reason of the appearance of the peak around $t_0 \approx 0$ can be understood by inspection of eq 19. In contrast to the excitation by a pump pulse with a small carrier frequency detuning, a large detuning of the pulse leads to the excitation of many higher-lying vibronic levels with small Franck−Condon factors. These levels possess high vibronic frequencies, so that the oscillating factors, $\exp\{i\omega^L_{\alpha n}t_0\}$, in eq 19 run rapidly out of phase. In the vicinity of $t_0 \approx 0$, however, all of the oscillatory terms are synchronized and the signal has a pronounced maximum. If the contribution from a particular pair of vibronic levels (α, n) dominates that from all other levels due to a favorable Franck−Condon factor, $V_{\alpha n}$, then several small-amplitude oscillations with the corresponding frequency, $\omega^L_{\alpha n}$, may show up in the cuts. In Figures 2c, 2f, and 3a, for example, a few low-amplitude beatings are seen following the peak at $t_0 \approx 0$, which correspond to $\omega^L_{\alpha n} = 4\ \Omega$.

The peak at $t_0 \approx 0$ is independent of the vibrational dissipation rate, and its shape is asymmetric. The left part ($t_0 < 0$) is determined by the square of the pump−pulse envelope, $\exp\{2\Gamma_L t_0\}$. The right part ($t_0 > 0$) depends on the OD rate. If $\xi_{eg} = 0$, then the peak falloff time is twice as long as the onset time. If the OD increases, then the falloff time decreases. Thus, analogously to what has been suggested in ref 22 and implemented in refs 34−36 for pump−probe signals, measurements of the TFG SE spectra with different pump−pulse durations allow for the estimation of the OD rate.

The peak at $t_0 \approx 0$ is reminiscent of the "coherent artifact", which occurs in optical signals when the pulses overlap.[22−43] An important difference has to be emphasized, however. The TFG SE spectra that are calculated within the generalized DW approximation via eq 19 are determined solely by the sequential contribution (15), and the height of the peak at $t_0 \approx 0$ depends on the carrier frequency detuning. The coherent spike in pump−probe spectra, however, is determined by both the sequential (pump precedes probe) and the coherent (probe precedes pump) contributions (see, for example, the discussion in ref 23). Moreover, the conditions for the appearance of the coherent spike in pump−probe spectra and the detuning-sensitive peak in TFG SE spectra are quite different and, in several respects, opposite. The coherent spike in pump−probe signals appears in the case of a large OD rate and also exists for small pump−pulse carrier-frequency detunings,[22,34−36] whereas the peak in

the TFG SE spectra described above exists only in the case of a small OD rate and moderate-to-large pump carrier-frequency detunings.

The inspection of Figures 2 and 3 reveals that the DW description requires a slippage of the initial condition[57−59] to ensure the coincidence of the DW and exact results at $t_0 > 1/\Gamma_L$. This observation may have important consequences if one tries to fit experimental TFG SE spectra within the DW approximation. If the OD is high enough and/or the pump−pulse carrier frequency detuning is small, then one can neglect the slippage safely and assume that the maximum of the actual signal coincides with the maximum of the signal calculated within the DW approximation. If, however, the OD is weak and/or the pump−pulse carrier frequency detuning is large, such an identification may lead to completely incorrect results (see Figures 2c, 2f, and 3a). In this case, the DW approximation can be used only to fit the signal at $t_0 > 1/\Gamma_L$.

3.2.2. Arbitrary Pump Pulse and Arbitrary Gate Pulse. Let us now relax the assumption of the previous section (neglect of the transient terms arising due to the finiteness of the gate pulse) and assume both the pump and the gate pulses to be of arbitrary duration. In contrast to the generalized DW approach, in which the signal is fully determined by the sequential contribution, taking into account all of the transient terms allows us to elucidate the significance of the coherent contributions to the TFG SE spectra.

The eigenvalue representation (eq 5) and the exponential pulse envelopes (eq 18) allow us to perform all of the time integrations in eqs 15 and 16 analytically.[60] The result reads:

$$S(t_0, \omega_0) = \sum_{\alpha,\beta;m,n} V_{\alpha n} V_{\alpha m} V_{\beta n} V_{\beta m} \rho_g^B(n)\, \Psi(x_2, y_2, x_1, y_1; t_0) + \sum_{\alpha,\beta;m,n} V_{\alpha n}^2 V_{\beta m}^2 \rho_g(n)\, \rho_e(\beta)[\Psi(-\xi_e, y_2, \xi_e, y_1; t_0) - \Psi(z_2, y_2, z_1, y_1; t_0)] \quad (20)$$

The TFG SE spectrum is seen to be determined uniquely by the quantity $\Psi(x_2, y_2, x_1, y_1; t_0)$, which is a function of the parameters

$$x_1 = i\omega_{\beta\alpha} + \nu_e + \xi_e \qquad y_1 = -\omega_{\beta n}^L - \xi_{eg} \qquad z_1 = \nu_e + \xi_e$$
$$x_2 = i\omega_{\alpha\beta} - \nu_e - \xi_e \qquad y_2 = i\omega_{\beta m}^0 - \xi_{eg} - \gamma \qquad z_2 = -\nu_e - \xi_e \quad (21)$$

(hereafter, the explicit dependence of $\Psi(t_0)$ on x_2, y_2, x_1, and y_1 is suppressed for simplicity of notation). The functions $\Psi(t_0)$ can be split into the sequential and coherent contributions, which, in turn, are determined by different expressions at positive and negative times:

$$\Psi(t_0) = \sum_{l=S,C} [\theta(-t_0)\, \Psi_-^l(t_0) + \theta(t_0)\, \Psi_+^l(t_0)] \quad (22)$$

The explicit time dependence of the quantities $\Psi_\pm^l(t_0)$ is the following (see also ref 4):

$$\Psi_+^S(t_0) = \Psi_{+1}^S \exp\{x_2 t_0\} + \Psi_{+2}^S \exp\{(y_1 - \Gamma_L)t_0\} + \Psi_{+3}^S \exp\{(y_2 - \Gamma)t_0\} + \Psi_{+4}^S \exp\{-2\Gamma_L t_0\} + \Psi_{+5}^S \exp\{-2\Gamma t_0\} \quad (23)$$

$$\Psi_-^S(t_0) = \Psi_{-1}^S \exp\{2\Gamma_L t_0\} + \Psi_{-2}^S \exp\{2\Gamma t_0\} \quad (24)$$

$$\Psi_+^C(t_0) = \Psi_{+1}^C \exp\{(x_2 - \Gamma - \Gamma_L)t_0\} + \Psi_{+2}^C \exp\{(y_1 - \Gamma_L)t_0\} + \Psi_{+3}^C \exp\{(y_2 - \Gamma)t_0\} + \Psi_{+4}^C \exp\{-2\Gamma_L t_0\} + \Psi_{+5}^C \exp\{-2\Gamma t_0\} \quad (25)$$

$$\Psi_-^C(t_0) = \Psi_{-1}^C \exp\{2\Gamma_L t_0\} + \Psi_{-2}^C \exp\{2\Gamma t_0\} + \Psi_{-3}^C \exp\{(x_2 + \Gamma + \Gamma_L)t_0\} \quad (26)$$

The Ψ_j^i coefficients are rather cumbersome algebraic functions of the parameters (21). These quantities are available analytically, but knowing their explicit form adds nothing profound to the present discussion. Much more important is the fact that eqs 23−26 give the explicit time-dependence of $\Psi(t_0)$, and thereby of the TFG SE spectrum.

Let us first consider sequential terms 23 and 24. Evidently, Ψ_{+1}^S represents the DW contribution to the TFG SE spectrum. All of the other terms may be regarded as transient terms because they decay with the characteristic times of the pump and gate pulses. These transient terms can be subdivided into two groups: those decaying monotonically and oscillatory, respectively. At positive times, the oscillatory terms decay as $\exp\{-\Gamma_L t_0\}$ or $\exp\{-\Gamma t_0\}$, whereas the monotonically decaying terms are damped twice as rapidly. At negative times, all of the terms decay monotonically. The onset of the signal is thus almost featureless, and the vibrational structure of the TFG SE spectrum at negative times is represented by the coherent terms (the contribution $\sim\Psi_{-3}^C$ in eq 26).

All of the terms constituting the coherent contribution, eqs 25 and 26, can be regarded as transient terms. As functions of time, both $\Psi_+^S(t_0)$ and $\Psi_+^C(t_0)$ have a similar structure (of course, the coefficients Ψ_j^S and Ψ_j^C depend on parameters (21) in a different way), except the terms Ψ_{+1}^C and Ψ_{-3}^C, which decay as $\exp\{-(\Gamma + \Gamma_L)|t_0|\}$. These contributions are unique in the sense that they describe a kind of interference between the pump and gate pulses and are negligible provided one of the two pulses is short enough. All of the other terms decay either with the characteristic time of the pump or the gate pulse.

As in the previous section, we first consider dissipation-free conditions ($\xi_{eg} = \nu_e = 0$). Figure 4 shows the sequential and coherent contributions (dashed and dot-dashed lines, respectively) as well as the total cut of the TFG SE spectrum (solid line) at the emission frequency $\omega_0 = \omega_L$, at which the coherent contribution reaches its maximum. The cuts in the upper (Figure 4a and c) and lower (Figure 4b and d) panels correspond to small ($\omega_L = 4\ \Omega$) and moderate ($\omega_L = 8\ \Omega$) carrier-frequency detuning of the pump pulse, respectively. The cuts in the left column (Figure 4a and b) have been computed for pump and gate pulses with the inverse durations $\Gamma_L = \Gamma = \Omega$. The cuts in the right column (Figure 4c and d) correspond to pulses that are three times longer, $\Gamma_L = \Gamma = {}^{\Omega}/_{3}$. The durations of the pulses, ${}^{1}/_{\Omega} = 33$ fs and ${}^{3}/_{\Omega} = 100$ fs, can nonetheless be regarded as rather short on the time scale of vibrational dynamics (${}^{2\pi}/_{\Omega} = 209$ fs).

When the pulses are short and the frequency detuning is small, the relative magnitudes of the sequential and coherent contributions in the vicinity of $t_0 \approx 0$ differ by a factor of 2 (Figure 4a). The presence of the coherent contribution does not change the behavior of the signal qualitatively. However, its significance grows dramatically with the increase of either the carrier-frequency detuning (Figure 4b) or the pulse durations (Figure 4c). The short time ($|t_0| < {}^{1}/_{\Gamma}$) evolution of the cuts in Figure 4b and c is seen to be dominated strongly by the coherent contribution and cannot be reproduced by the sequential one.

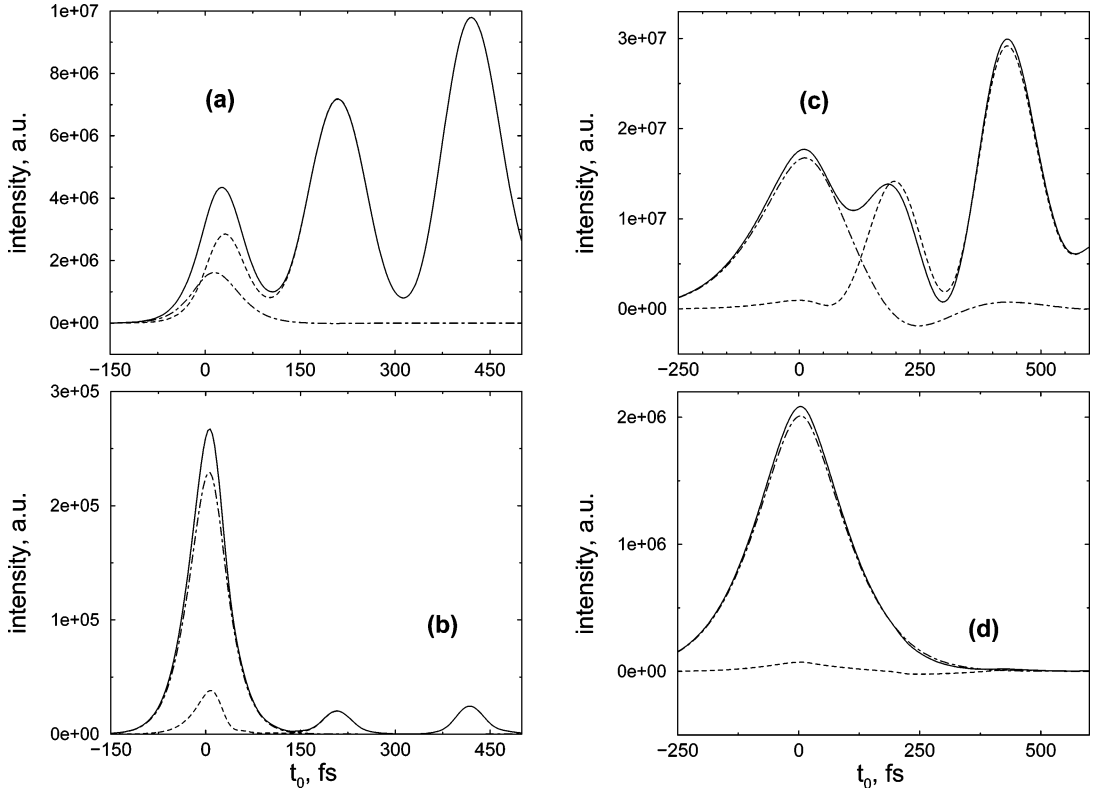

Figure 4. Cuts of the TFG SE spectrum at $\omega_0 = \omega_L$, calculated neglecting dissipative effects ($\nu_e = \xi_{eg} = 0$). The inverse durations of the pump and gate pulses are $\Gamma_L = \Gamma = \Omega$ in a and b, and $\Gamma_L = \Gamma = {}^{\Omega}/_{3}$ in c and d. The upper and lower panels correspond to small and moderate detunings, respectively ($\omega_L = 4\ \Omega$ in a and c and $\omega_L = 8\ \Omega$ in b and d). The signal is shown by the solid line, whereas the sequential and coherent contributions are represented by the dashed and dotted-dashed lines, respectively.

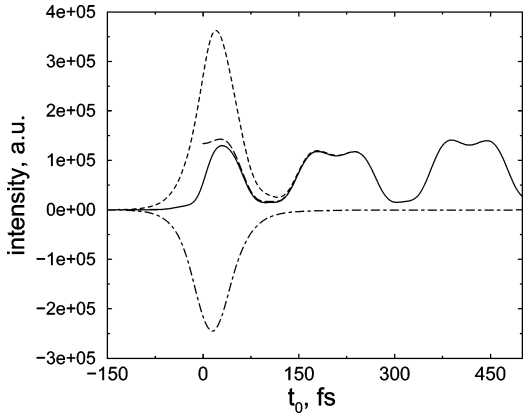

Figure 5. Cut of the TFG SE spectrum at $\omega_0 = 3.5\ \Omega$ for short pump and gate pulses ($\Gamma_L = \Gamma = \Omega$), moderate detuning ($\omega_L = 8\ \Omega$), calculated neglecting dissipative effects ($\nu_e = \xi_{eg} = 0$). The signal is shown by the solid line, whereas the sequential and coherent contributions are represented by the dashed and dotted-dashed lines, respectively. The standard DW result is indicated by the long-dashed line.

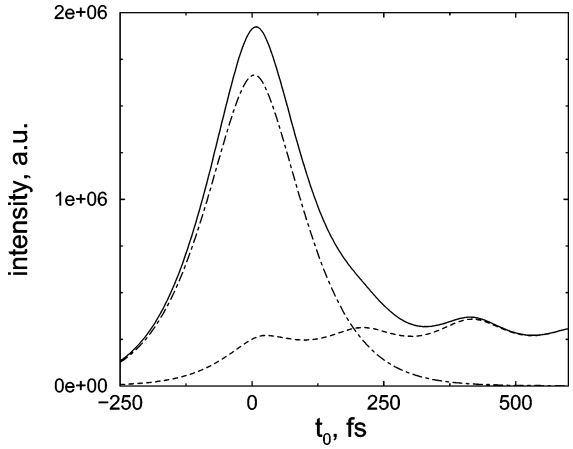

Figure 6. Cut of the TFG SE spectrum at $\omega_0 = \omega_L$, calculated with relatively long pump and gate pulses ($\Gamma_L = \Gamma = {}^{\Omega}/_{3}$), moderate detuning ($\omega_L = 8\ \Omega$) and OD rate $\xi_{eg} = \Omega$. Vibrational relaxation is not taken into account ($\nu_e = 0$). The signal is shown by the solid line, whereas the sequential and coherent contributions are represented by the dashed and dotted-dashed lines, respectively.

If both the pulse durations and the frequency detuning increase, then the coherent contribution determines the cut almost solely (Figure 4d). Thus, in contrast to pump−probe spectra,[42] the neglect of contributions due to overlapping pulses may not only overestimate but also substantially underestimate the TFG SE signal at short times.

The coherent contribution can become substantial not only in the positive domain but also in the negative domain. Figure 5 depicts the cuts at $\omega_0 = 3.5\ \Omega$, which are computed with short pump and gate pulses ($\Gamma_L = \Gamma = \Omega$) and moderate detuning ($\omega_L = 8\ \Omega$). The coherent and sequential contributions at $|t_0| < {}^{1}/_{\Gamma}$ are seen to have almost the same magnitudes but opposite signs. Interestingly, the total cut coincides almost completely with its DW counterpart at $t_0 > 0$. As is clearly seen from Figure 6, this is caused by the cancellation of two large correction terms.

As has been demonstrated in the previous section, the major effect of vibrational relaxation on the TFG SE spectrum is the overall reduction of the signal intensity. The role of OD, however, is more intriguing. It is well known for steady-state SE spectra that the widths of the Raman lines, in contrast to the fluorescence lines, are almost unaffected by the OD. However, the increase of OD redistributes the SE intensity to the fluorescence at the expense of the Raman contribution.[2] In the time domain, the situation is rather different. As is clearly

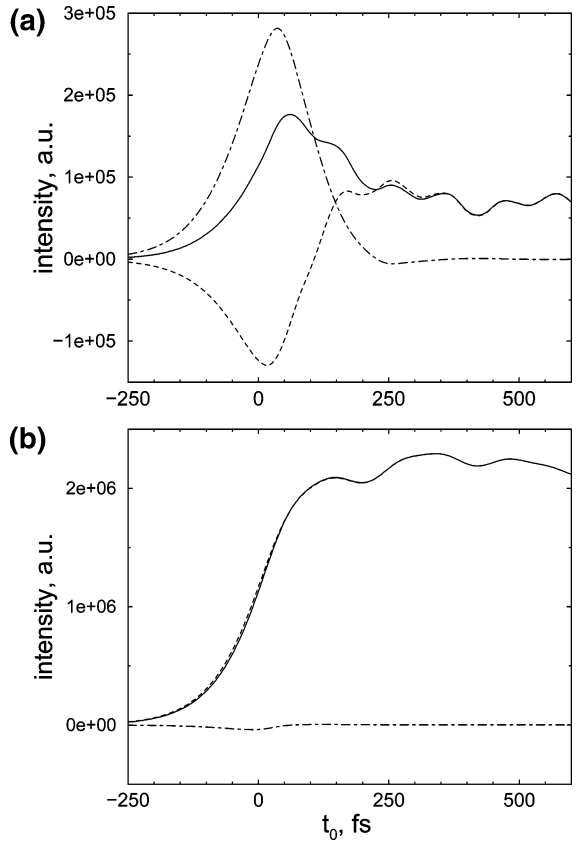

Figure 7. Cuts of the TFG SE spectrum at $\omega_0 = 0.8\ \Omega$, calculated with the same pump- and gate-pulse parameters as in Figure 6. (a) $\xi_{eg} = 0$; (b) $\xi_{eg} = \Omega$. Vibrational relaxation is not taken into account ($\nu_e = 0$). The signal is shown by the solid line, whereas the sequential and coherent contributions are represented by the dashed and dotted-dashed lines, respectively.

seen from eqs 23−26, some of the Ψ^{I}_{+q} terms are proportional to $\exp\{-\xi_{eg}t_0\}$, whereas the others are independent of the OD rate. Thus, in every particular case, the significance of the influence of the OD is determined by the relative importance of these two kinds of terms.

To illustrate this statement, we present several cuts of the TFG SE spectrum calculated for pump and gate pulses with $\Gamma_L = \Gamma = {}^{\Omega}/_{3}$ and moderate detuning ($\omega_L = 8\ \Omega$). The vibrational relaxation has been neglected ($\nu_e = 0$). The cut at $\omega_0 = \omega_L$ computed with a moderate OD ($\xi_{eg} = \Omega$) is shown in Figure 6. The comparison of this cut with its counterpart calculated with $\xi_{eg} = 0$ (Figure 4d) does not reveal a substantial effect of the OD on the coherent contribution, whereas the role of the sequential contribution increases. A completely different situation is presented in Figure 7 showing the cuts at $\omega_0 = 0.8\ \Omega$ calculated without OD (a, $\xi_{eg} = 0$) and with a moderate OD (b, $\xi_{eg} = \Omega$). The influence of the OD on the coherent contribution is seen to be enormous: it practically disappears. Parenthetically, the sequential contribution in Figure 7a attains negative values, which is a rather unexpected finding.

Note finally that if the pump and gate pulses are (much) longer than the system vibrational period, then the sequential and coherent contributions (and thus the TFG SE spectrum itself) depend significantly not only on the magnitude of the pump carrier frequency detuning but also on whether the carrier frequency is in resonance with a particular transition to a vibronic level of the optically bright state (see, for example, refs 5, 16, and 21).

4. Conclusions

We have explored the short-time behavior of TFG SE spectra, when the pump and gate pulses overlap and their durations are shorter than or comparable with the time scale of the system dynamics. A model of the material dynamics that accounts for strong nonadiabatic and electron−vibrational coupling effects as well as for dissipative effects has been chosen to represent generic photoinduced excited-state dynamics in large molecules in the gas phase or in condensed phases. The analysis has been carried out analytically by the incorporation of a phenomenological relaxation model[44] into the generalized DW framework[16] and beyond. The present approach allowed us to single out the sequential and coherent contributions, as well as the DW-contribution, to the TFG SE spectrum and to study their dependence on pump and gate pulse carrier frequencies and durations, vibrational relaxation, and the OD rate separately.

If the temporal resolution is perfect and the coherent contribution can thus be neglected, then the TFG SE spectra excited with moderate or large frequency detuning have been shown to exhibit a pronounced feature centered at zero gate-pulse delay, provided the OD is weak. This peak is caused exclusively by the sequential (pump precedes gate) contribution to the TFG SE spectrum. This phenomenon cannot be reproduced within the standard DW approximation, implying that the validity of the latter depends on the pump−pulse carrier frequency detuning.

If both the pump and gate pulses are short on the time scale of the system dynamics, then the interplay between the sequential and coherent contributions to the TFG SE has been found to be very sensitive to the pump−pulse carrier-frequency detuning and the OD rate. This fact allows, in principle, the experimental determination of the OD rate. It has been shown that the coherent contribution dominates the TFG SE spectrum at specific SE frequencies.

Acknowledgment. This work has been supported by the Deutsche Forschungsgemeinschaft and the Fonds der Chemischen Industrie. M.F.G. acknowledges support by an Alexander von Humboldt research fellowship. We are grateful to Andrey Kazansky for his interest in this work and useful discussions.

Appendix A

As has been demonstrated in ref 44, the third-order optical response functions of a dissipative material system can be expressed through those of the corresponding bath-free system. Explicitly[64]

$$R_1(t_3, t_2, t_1) = \exp\{-\xi_{eg}(t_1 + t_3) - \xi_e t_2\} \times [R_1(t_3, t_2, t_1)^{fr} \exp\{-\nu_e t_2\} + J_g(t_1)J_e(t_3)(1 - \exp\{-\nu_e t_2\})] \quad \text{(A1)}$$

$$R_2(t_3, t_2, t_1) = \exp\{-\xi_{eg}(t_1 + t_3) - \xi_e t_2\} \times [R_2(t_3, t_2, t_1)^{fr} \exp\{-\nu_e t_2\} + J^*_g(t_1)J_e(t_3)(1 - \exp\{-\nu_e t_2\})] \quad \text{(A2)}$$

$$R_3(t_3, t_2, t_1) = \exp\{-\xi_{eg}(t_1 + t_3)\} \times [R_3(t_3, t_2, t_1)^{fr} \exp\{-\nu_g t_2\} + J^*_g(t_1)J_g(t_3)(1 - \exp\{-\nu_g t_2\})] \quad \text{(A3)}$$

The excited-state population decay rate, ξ_e, the OD rate, ξ_{eg}, and the vibrational relaxation rates, ν_a (a = e, g), have been

defined in eqs 10 and 11. The third-order bath-free optical response functions are defined explicitly as usual:[2]

$$R_1^{\mathrm{fr}}(t_3, t_2, t_1) = Tr[\exp\{\mathrm{i}H_g t_1\}V_{ge}\exp\{\mathrm{i}H_e t_2\}V_{eg} \exp\{\mathrm{i}H_g t_3\}V_{ge}\exp\{-\mathrm{i}H_e(t_1+t_2+t_3)\}V_{eg}\rho_g] \quad \text{(A4)}$$

$$R_2^{\mathrm{fr}}(t_3, t_2, t_1) = Tr[V_{ge}\exp\{\mathrm{i}H_e(t_1+t_2)\}V_{eg} \exp\{\mathrm{i}H_g t_3\}V_{ge}\exp\{-\mathrm{i}H_e(t_2+t_3)\}V_{eg}\exp\{-\mathrm{i}H_g t_1\}\rho_g], \quad \text{(A5)}$$

$$R_3^{\mathrm{fr}}(t_3, t_2, t_1) = Tr[V_{ge}\exp\{\mathrm{i}H_e t_1\}V_{eg} \exp\{\mathrm{i}H_g(t_2+t_3)\}V_{ge}\exp\{-\mathrm{i}H_e t_3\}V_{eg}\exp\{-\mathrm{i}H_g(t_1+t_2)\}\rho_g] \quad \text{(A6)}$$

The quantities

$$J_g(t) = Tr[\exp\{\mathrm{i}H_g t\}V_{ge}\exp\{-\mathrm{i}H_e t\}V_{eg}\rho_g] \quad \text{(A7)}$$

and

$$J_e(t) = Tr[\exp\{\mathrm{i}H_e t\}V_{eg}\exp\{-\mathrm{i}H_g t\}V_{ge}\rho_e] \quad \text{(A8)}$$

are the first-order optical response functions, the Fourier transforms of which represent the linear absorption and relaxed fluorescence spectra, respectively.[2] The Boltzmann operators ρ_a(a = e,g) are defined in eq 13.

Appendix B

Let us neglect the transient terms decaying with the characteristic time of the gate pulse, while keeping all the transient terms decaying with the characteristic time of the pump pulse. In doing so, one arrives at the generalized DW approximation. In that case, as has been demonstrated in ref 16, one can drop the coherent contribution (16) to the TFG SE spectrum and put $t = 0$ in the upper integration limit over t_2 in eq 15. We additionally assume that the gate pulse is short on the time scale of vibrational dynamics and relaxation, thereby implying that the time resolution is perfect. This allows us to put $t = 0$ everywhere under the integral sign in eq 15. A straightforward analysis then shows that the TFG SE spectrum can be represented as the sum of "free" and "relaxed" contributions (compare with ref 44):

$$S(t_0, \omega_0) \approx Tr[W^{\mathrm{fr}}(\omega_0)G^{\mathrm{fr}}(t_0)D^{\mathrm{fr}}(t_0,\omega_L)] + W^{\mathrm{rel}}(\omega_0)G_1^{\mathrm{rel}}(t_0)D_1^{\mathrm{rel}}(t_0, \omega_L) - W^{\mathrm{rel}}(\omega_0)G_2^{\mathrm{rel}}(t_0)D_2^{\mathrm{rel}}(t_0, \omega_L) \quad \text{(B1)}$$

Here, the generalized D operator and the W operator are determined via the expressions

$$D^j(t_0, \omega_L) = \int_{-\infty}^{t_0} \mathrm{d}t_2 \int_0^{\infty} \mathrm{d}t_1\, E_L(t_2)\, E_L(t_2 - t_1) \exp\{(\mathrm{i}\omega_L - \xi_{eg})t_1 + \xi_e t_2\}D^j(t_2, t_1) + H.c. \quad \text{(B2)}$$

$$W^j(\omega_0) = \int_0^{\infty} \mathrm{d}t_3\, E_t(t_3)\exp\{(\mathrm{i}\omega_0 - \gamma - \xi_{eg})t_1\}W^j(t_3) + H.c. \quad \text{(B3)}$$

in which

$$D^{\mathrm{fr}}(t_2, t_1) = \mathrm{e}^{(\mathrm{i}H_e + \nu_e)t_2}\mathrm{e}^{-\mathrm{i}H_e t_1}V_{eg}\rho_g^{\mathrm{eq}}\mathrm{e}^{\mathrm{i}H_g t_1}V_{ge}\mathrm{e}^{-\mathrm{i}H_e t_2} \quad \text{(B4)}$$

$$W^{\mathrm{fr}}(t_3) = V_{eg}\mathrm{e}^{\mathrm{i}H_g t_3}V_{ge}\mathrm{e}^{-\mathrm{i}H_e t_3} \quad \text{(B5)}$$

$$D_1^{\mathrm{rel}}(t_2, t_1) = J_g(t_1) \qquad D_2^{\mathrm{rel}}(t_2, t_1) = e^{\nu_e t_2}J_g(t_1) \quad \text{(B6)}$$

$$W^{\mathrm{rel}}(t_3) = J_e(t_3) \quad \text{(B7)}$$

The excited-state propagators are defined as follows:

$$G^{\mathrm{fr}}(t_0)X = \mathrm{e}^{-\mathrm{i}H_e t_0}X\mathrm{e}^{\mathrm{i}H_e t_0}\mathrm{e}^{-(\nu_e+\xi_e)t_0}\ \forall X \quad \text{(B8)}$$

$$G_1^{\mathrm{rel}}(t_0)X = \mathrm{e}^{-\xi_e t_0}X \qquad G_2^{\mathrm{rel}}(t_0)X = \mathrm{e}^{-(\nu_e+\xi_e)t_0}X\ \forall X \quad \text{(B9)}$$

In the derivation of the above expressions, we did take account of bath-induced vibrational relaxation during the pump pulse. The free and relaxed W functions (B5) and (B7) are time-independent and are identical with their standard counterparts.[44] The generalized D functions (B4) and (B6), however, are t_0-dependent. They reduce to their conventional analogues in the limit of well-separated pump and gate pulses.[44]

Adopting the eigenvalue representation for the ground- and excited-state Hamiltonians (5) and using the exponential pulse envelopes (18), one can perform all of the time integrals in eqs B2 and B3 analytically[65] with the result

$$S(t_0, \omega_0) = \sum_{\alpha,\beta}\exp\{-(\mathrm{i}\omega_{\alpha\beta} + \nu_e + \xi_e)t_0\} D_{\alpha\beta}(t_0, \nu_e + \xi_e)\, W_{\alpha\beta}(\omega_0) + \exp\{-\xi_e t_0\} \sum_{\alpha}\{D_{\alpha\alpha}(t_0, \xi_e) - \exp\{-\nu_e t_0\}D_{\alpha\alpha}(t_0, \nu_e + \xi_e)\}W(\omega_0) \quad \text{(B10)}$$

The generalized time-dependent D function

$$D_{\alpha\beta}(t, y) \equiv \sum_n V_{\alpha n}V_{n\beta}\rho_g^{\mathrm{B}}(n)\{\theta(-t)\Phi_{\alpha\beta;n}^{-}(t, y) + \theta(t)\Phi_{\alpha\beta;n}^{+}(t, y)\} \quad \text{(B11)}$$

($\theta(t)$ is the Heaviside step function) is explicitly defined as follows:

$$\Phi_{\alpha\beta;n}^{-}(t, y) = \frac{\exp\{(2\Gamma_L + y + \mathrm{i}\omega_{\alpha\beta})t\}}{(2\Gamma_L + y + \mathrm{i}\omega_{\alpha\beta})(\bar{\Gamma}_L - \mathrm{i}\omega_{\alpha n}^{L})} + H.c. \quad \text{(B12)}$$

$$\Phi_{\alpha\beta;n}^{+}(t, y) = \frac{1}{(2\Gamma_L + y + \mathrm{i}\omega_{\alpha\beta})(\bar{\Gamma}_L - \mathrm{i}\omega_{\alpha n}^{L})} + \frac{1 - \exp\{-(\bar{\Gamma}_L - y - \mathrm{i}\omega_{\beta n}^{L})t\}}{\bar{\Gamma}_L - y - \mathrm{i}\omega_{\beta n}^{L}} \times \left\{\frac{1}{\bar{\Gamma}_L - \mathrm{i}\omega_{\alpha n}^{L}} + \frac{1}{2\Gamma_L - y - \mathrm{i}\omega_{\alpha\beta}}\right\} - \frac{\exp\{-(\bar{\Gamma}_L - y - \mathrm{i}\omega_{\beta n}^{L})t\}(1 - \exp\{-(\Gamma_L - \xi_{eg} + \mathrm{i}\omega_{\alpha n}^{L})t\})}{(2\Gamma_L - y - \mathrm{i}\omega_{\alpha\beta})(\Gamma_L - \xi_{eg} + \mathrm{i}\omega_{\alpha n}^{L})} + H.c. \quad \text{(B13)}$$

The W functions are defined through the quantity

$$\Psi_{\alpha\beta}(\omega_0) = \left\{\frac{\Gamma}{\Gamma - \mathrm{i}\omega_{\alpha n}^{0}} + \frac{\Gamma}{\Gamma - \mathrm{i}\omega_{\beta n}^{0}}\right\} + H.c.$$

as

$$W_{\alpha\beta}(\omega_0) = \sum_n V_{\alpha n} V_{n\beta} \Psi_{\alpha\beta}(\omega_0)$$

$$W(\omega_0) = \sum_{\alpha;n} V_{\alpha n}^2 \Psi_{\alpha\alpha}(\omega_0)\, \rho_e^B(\alpha) \quad \text{(B14)}$$

Thus, the choice of the exponential gate-pulse envelope (18) gives rise to simple Lorentzian SE line shapes. The Boltzmann factors are written as

$$\rho_g^B(n) = Z_g^{-1} \exp\left\{\frac{-\epsilon_n}{kT}\right\} \qquad \rho_e^B(\alpha) = Z_e^{-1} \exp\left\{\frac{-\epsilon_\alpha}{kT}\right\} \quad \text{(B15)}$$

and the rest of the parameters are defined as follows:

$$\bar{\Gamma}_L \equiv \Gamma_L + \xi_{eg} \qquad \omega_{\alpha n}^L \equiv \omega_L - \omega_{\alpha n} \qquad \omega_{\alpha n}^0 \equiv \omega_0 - \omega_{\alpha n} \quad \text{(B16)}$$

The above expressions generalize those derived in ref 44 because we (i) account for the transient terms, (ii) do include dissipation during the pump pulse, and (iii) calculate the TFG SE signal at an arbitrary time $-\infty < t_0 < \infty$.

Inspection of eqs B12 and B13 reveals the following. Equation B12 describes the only contribution that exists at negative times, during the build up of the TFG SE signal. The onset of the signal is featureless and monotonic because it is described by the factor $\theta(-t_0)\exp\{2\Gamma_L t_0\}$. The term B12 reaches its maximum at $t_0 = 0$ and constitutes one of the contributions to the standard D function at positive times (the first term in eq B13). All of the other contributions to eq B13 are identically zero at $t_0 = 0$ and exist only for positive times. They consist of time-independent terms (which enter the standard D function) and transient terms.

It is important to note that the TFG SE signal reaches its maximum not at $t_0 = 0$ (which corresponds to the maximum of the excitation pulse, $E_L(t_0)$) but at a later time. Indeed, the time derivative of the generalized D function (45) at $t_0 = +0$ is proportional to $\bar{\Gamma}_L/(\bar{\Gamma}_L^2 + (\omega_{\alpha n}^L)^2) > 0$. Thus, as has been demonstrated in ref 4 for three-level systems, the TFG SE signal keeps growing after the excitation pulse has reached its maximum. This conclusion is not a consequence of the specific dissipation model employed. It holds even in the bath-free case ($\nu_e = \xi_{eg} = 0$). The same applies also to pump−probe signals.[22,34,36,37]

The explicit expression for the frequency-integrated SE signal, $S(t_0)$, is also given by eq B10 in which one has to substitute

$$W_{\alpha\beta}(\omega_0) \rightarrow W_{\alpha\beta} = \sum_n V_{\alpha n} V_{n\beta}$$

$$W(\omega_0) \rightarrow W = \sum_{\alpha;n} V_{\alpha n}^2\, \rho_e^B(\alpha) \quad \text{(B17)}$$

As is easy to verify, the frequency-integrated SE signal determined in this way is connected with the "exact" one, $S_t(t_0)$ (which is obtained by direct integration of eq 15 and is thus valid for any gate-pulse duration and at any t_0), by a simple convolution:

$$S_t(t_0) = \int_{-\infty}^{\infty} dt\, E_t^2(t_0 - t) S(t) \quad \text{(B18)}$$

Note, finally, that a very similar analysis can be carried out for pump−probe spectra, as outlined in ref 67.

References and Notes

(1) Yan, Y. J.; Mukamel, S. *J. Chem. Phys.* **1987**, *86*, 6085.
(2) Mukamel, S. *Principles of Nonlinear Optical Spectroscopy*; Oxford University Press: Oxford, U.K., 1995.
(3) Rousseau, D. L.; Williams, P. F. *J. Chem. Phys.* **1976**, *64*, 3525.
(4) Melinger, J. S.; Albrecht, A. C. *J. Chem. Phys.* **1986**, *84*, 1247.
(5) Williams, S. O.; Imre, D. G. *J. Chem. Phys.* **1988**, *92*, 3363.
(6) Shapiro, M. *J. Chem. Phys.* **1993**, *99*, 2453.
(7) Ungar, L. W.; Cina, J. A. *Adv. Chem. Phys.* **1997**, *100*, 171.
(8) Domcke, W.; Stock, G. *Adv. Chem. Phys.* **1997**, *100*, 1.
(9) Eberly, J. H.; Wodkiewicz, K. *J. Opt. Soc. Am.* **1977**, *67*, 1253.
(10) Schanz, R.; Kovalenko, S. A.; Kharlanov, V.; Ernsting, N. P. *Appl. Phys. Lett.* **2001**, *79*, 566.
(11) Kowalczyk, P.; Radzewicz, C.; Mostowski, J.; Walmsley, I. A. *Phys. Rev. A* **1990**, *42*, 5622.
(12) Waxer, L. J.; Walmsley, I. A.; Vogel, W. *Phys. Rev. A* **1997**, *56*, R2491.
(13) Santoro, F.; Petrongolo, C.; Lami, A. *J. Chem. Phys.* **2000**, *113*, 4073.
(14) Mukamel, S. *J. Chem. Phys.* **1997**, *107*, 4165.
(15) Gelin, M. F.; Pisliakov, A. V.; Domcke, W. *Phys. Rev. A* **2002**, *65*, 062507.
(16) Gelin, M. F.; Egorova, D.; Pisliakov, A. V.; Domcke, W. *Chem. Phys. Lett.* **2004**, *391*, 234.
(17) Rosenthal, S. J.; Xie, X.; Du, M.; Fleming, G. R. *J. Chem. Phys.* **1991**, *95*, 4715.
(18) Jimenez, R.; Fleming, G. R.; Kumar, P. V.; Maroncelli, M. *Nature* **1994**, *369*, 471.
(19) Rubtsov, I. V.; Yoshihara, K. *J. Phys. Chem. A* **1999**, *103*, 10202.
(20) Rubtsov, I. V.; Yoshihara, K. In *Femtochemistry*; De Schryver, F. C., De Feyter, S., Schweiteret, G., Eds.; Wiley: Berlin, 2001.
(21) Gelin, M. F.; Egorova, D.; Domcke, W. *J. Chem. Phys.*, in press.
(22) Balk, M. W.; Fleming, G. R. *J. Chem. Phys.* **1985**, *83*, 4300.
(23) Joo, T.; Jia, Y.; Yu, J.; Lang, M. J.; Fleming, G. R. *J. Chem. Phys.* **1996**, *104*, 6089.
(24) Larsen, D. S.; Ohta, K.; Xu, Q.; Cyrier, M.; Fleming, G. R. *J. Chem. Phys.* **2001**, *114*, 8008.
(25) Ohta, K.; Larsen, D. S.; Yang, M.; Fleming, G. R. *J. Chem. Phys.* **2001**, *114*, 8020.
(26) Walmsley, I. A.; Mitsunaga, M.; Tang, C. L. *Phys. Rev. A* **1988**, *38*, 4681.
(27) Pollard, W. T.; Brito Cruz, C. H.; Shank, C. V.; Mathies, R. A. *J. Chem. Phys.* **1989**, *90*, 199.
(28) Pollard, W. T.; Dexheimer, S. L.; Wang, O.; Petanu, L. A.; Shank, C. V.; Mathies, R. A. *J. Chem. Phys.* **1992**, *96*, 6147.
(29) Ferwerda, H. A.; Terpstra, J.; Wiersma, D. A. *J. Chem. Phys.* **1989**, *91*, 3296.
(30) Duppen, K.; Haan, F.; Niberring, E. T. J.; Wiersma, D. A. *Phys. Rev. A* **1993**, *47*, 5120.
(31) Boyd, R. W.; Mukamel, S. *Phys. Rev. A* **1984**, *29*, 1973.
(32) Yan, Y. J.; Fried, L. E.; Mukamel, S. *J. Phys. Chem.* **1989**, *93*, 8149.
(33) Kang, T. J.; Yu, J.; Berg, M. *J. Chem. Phys.* **1991**, *94*, 2413.
(34) Cong, P.; Deuel, H. P.; Simon, J. D. *Chem. Phys. Lett.* **1993**, *212*, 367.
(35) Cong, P.; Yan, Y. J.; Deuel, H. P.; Simon, J. D. *J. Chem. Phys.* **1994**, *100*, 7855.
(36) Chachisvilis, M.; Fidder, H.; Sundström, V. *Chem. Phys. Lett.* **1995**, *234*, 141.
(37) Chachisvilis, M.; Sundström, V. *J. Chem. Phys.* **1996**, *104*, 5734.
(38) Che, J.; Zhang, W.; Yan, Y. J. *J. Chem. Phys.* **1997**, *106*, 6947.
(39) Fain, B., Lin, S. H.; Khidekel, V. *Phys. Rev. A* **1993**, *47*, 3222.
(40) Kovalenko, S. A.; Dobryakov, A. L.; Ruthmann, J.; Ernsting, N. P. *Phys. Rev. A* **1999**, *59*, 2369.
(41) Dobryakov, A. L.; Kovalenko, S. A.; Ernsting, N. P. *J. Chem. Phys.* **2003**, *119*, 988.
(42) Shen, Y.-C.; Cina, J. A. *J. Chem. Phys.* **1999**, *110*, 9793.
(43) Farrow, D. A.; Yu, A.; Jonas, D. M. *J. Chem. Phys.* **2003**, *118*, 9348. Farrow, D. A.; Yu, A.; Jonas, D. M. *J. Chem. Phys.* **2003**, *119*, 4599.
(44) Gelin, M. F.; Pisliakov, A. V.; Egorova, D.; Domcke, W. *J. Chem. Phys.* **2003**, *118*, 5287.
(45) Hayashi, M.; Yang, T.-S.; Yu, J.; Mebel, A.; Lin, S. H. *J. Phys. Chem. A* **1997**, *101*, 4156.
(46) Hayashi, M.; Yang, T.-S.; Yu, J.; Mebel, A.; Chang, R.; Lin, S. H.; Rubtsov, I. V.; Yoshihara, K. *J. Phys. Chem. A* **1998**, *102*, 4256.
(47) Pisliakov, A. V.; Gelin, M. F.; Domcke, W. In *Femtochemistry and Femtobiology*; Martin, M. M., Hynes, J. T., Eds.; Elsevier: Amsterdam, 2004; p 303.
(48) Note that, to good accuracy, dissipation effects during the pump pulse can be neglected. For the system under study, the TFG SE spectra calculated for $\nu_e = \Omega/3$ with and without this assumption are indistinguishable (not shown).
(49) Jean, J. M.; Friesner, R. A.; Fleming, G. R. *J. Chem. Phys.* **1992**, *96*, 5827.

(50) Ashkenazi, G.; Kosloff, R.; Ratner, M. A. *J. Am. Chem. Soc.* **1999**, *121*, 3386.
(51) Kosloff, R.; Ratner, M. A. *J. Phys. Chem. B* **2002**, *106*, 8479.
(52) Coch, C. P.; Klüner, T.; Kosloff, R. *J. Chem. Phys.* **2002**, *116*, 7983.
(53) Lockwood, D. M.; Ratner, M. A.; Kosloff, R. *J. Chem. Phys.* **2002**, *117*, 10125.
(54) Parson, W. W.; Warshel, A. *Chem. Phys.* **2004**, *296*, 201.
(55) Prezhdo, O. V. *Phys. Rev. Lett.* **2000**, *85*, 4413.
(56) Williams, S. O.; Imre, D. G. *J. Phys. Chem.* **1988**, *92*, 6648.
(57) Suarez, A.; Silbey, R.; Oppenheim, I. *J. Chem. Phys.* **1992**, *97*, 5101.
(58) Gaspard, P.; Nagaoka, M. *J. Chem. Phys.* **1999**, *111*, 5668.
(59) Mančal, T.; May, V. *J. Chem. Phys.* **2001**, *114*, 1510.
(60) From the computational point of view, it is more efficient to calculate the TFG SE spectrum starting, for example, from eq 2.18 of paper,[7] in which there is no separation of the SE into S and C components. In doing so, one can represent the TFG SE spectrum as a sum of squares of particular amplitudes (see also ref 8). Our aim is, however, to study the behavior of the S and C components separately.
(61) Jonas, D. M.; Bradforth, S. E.; Passino, S. A.; Fleming, G. R. *J. Phys. Chem.* **1995**, *99*, 2594.
(62) Jean, J. M. *J. Chem. Phys.* **1994**, *101*, 10464.
(63) Kumar, A. T. N.; Rosca, F.; Widom, A.; Champion, P. M. *J. Chem. Phys.* **2001**, *114*, 701.
(64) Note a misprint in ref 44: In eqs 19 and 20 of that paper, one must replace $J_e(t_3)$ with $J_g(t_3)$.
(65) If Gaussian pulse envelopes are used, the results can be expressed in terms of complex error functions; compare with refs 7, 42, and 66.
(66) Balzer, B.; Stock, G. *J. Phys. Chem. A* **2004**, *108*, 6464.
(67) Gelin, M. F.; Pisliakov, A. V.; Domcke, W. In *Femtochemistry and Femtobiology*; Martin, M. M., Hynes, J. T., Eds.; Elsevier: Amsterdam, 2004; p 311.